

# Space-time non-separable dynamics of ultrashort vortex pulse with power exponential spectrum

Shakti Singh<sup>1</sup> and Akhilesh Kumar Mishra<sup>1,2,\*</sup>

<sup>1</sup>*Department of Physics, Indian Institute of Technology Roorkee, Roorkee-247667, Uttarakhand, India*

<sup>2</sup>*Centre for Photonics and Quantum Communication Technology, Indian Institute of Technology Roorkee,*

*\*Corresponding author [akhilesh.mishra@ph.iitr.ac.in](mailto:akhilesh.mishra@ph.iitr.ac.in)*

**Abstract:** Ultrashort optical pulses with orbital angular momentum (OAM) owing to their various applications in classical as well as quantum domains attract a lot of research attention. The evolution of their spatio-temporal dynamics is of particular interest. In the present work, we numerically explore the spatio-temporal evolution of ultrashort Laguerre Gauss (LG) vortex with power exponential spectrum, also called power exponential (PE) pulse, in dispersive and nonlinear media. We in particular address the evolution of space-time non-separable ultrashort vortex pulse. The study reveals the asymmetric spatio-temporal evolution and splitting in the spatio-temporal plane. We observe compression at the trailing edge of the pulse with increase in the strength of the nonlinearity. The study further reveals that the temporal, spectral and, chirp evolution patterns of the pulse vary uniquely across different spatial regions and this variation depends upon the strength of nonlinearity and propagation distance. In weak nonlinear regime, a redshift in spectrum is noted as we move radially outward from the bright caustic of ultrashort LG vortex while a blue shifted spectrum emerges on approaching towards the phase singularity. Interestingly, as the pulse furthers in the medium, nonlinearity induced trends in spectral shift is witnessed. With stronger nonlinearity, a complex spectral evolution is observed. Furthermore, we study the evolution of frequency chirp with propagation distance both with weak and strong nonlinearities.

## 1. Introduction:

Ever since the advent of ultrafast laser sources, due to their unprecedented properties and related applications the field of ultrafast optics has witnessed continuing research interest. The ultrashort pulses have found significant attention across various research areas such as metamaterials [1], communications [2], particle acceleration [3], laser machining [4], nonlinear and topological photonics [5] to name a few. In these mentioned applications, it is important to precisely control the shape of optical pulses not only in time but in space as well. Consequently, recent years have witnessed a growing interest in understanding the dynamics of optical pulses in both the dimensions.

Generally, optical pulses in factorized solution of the Maxwell's equations are treated as space time separable solution, where a pulse can be expressed as product of spatial function and temporal function. However, this assumption does not hold good in ultrafast regime and hence a non-separable space-time solution was proposed [6]. In ultrafast domain, optical pulses exhibit a correlation between spatial and temporal degrees of freedom, known as spatio-temporal coupling [7]. The consequence of spatio-temporal coupling leads to emergence of phenomena such as iso-diffraction and iso-divergence [8]. In ultrashort pulse, the spatio-temporal coupling results phenomenal effects such as red shift in the spectrum, time dependent diffraction, space dependent pulse time delay etc [9–11].

Since the first realization that Laguerre Gauss (LG) beam with azimuthal integer  $l$  carries an orbital angular momentum (OAM) of  $l\hbar$  per photon, the exploration of light carrying OAM has surged in recent years [12–14]. Light with OAM exhibits undefined phase at its centre called phase singularity. Light with OAM finds applications in various field such as optical communication [15], micromanipulation [16], phase-contrast microscopy [17], and quantum information processing [18] among others.

In recent years, ultrashort pulses with OAM (also known as ultrashort vortices) have also been investigated theoretically as well as experimentally [19–21]. As stated earlier ultrashort pulses exhibit spatio-temporal coupling. While ultrashort vortices possess additional coupling between OAM degree of freedom and temporal degree of freedom due to which temporal shape strongly depends upon OAM [22,23]. The temporal-OAM coupling is a special case of spatio-temporal coupling. Researcher have been familiar with spatio-temporal coupling of the wave equation solutions for decades. Typically, these couplings are small in ultrashort pulses without OAM [24]. However, it can be amplified for specific applications artificially [7]. In ultrashort vortices,

high intense spatial regions and low intense spatial regions exist and temporal-OAM coupling varies considerably in these spatial regions [22]. Recently, it has been demonstrated theoretically that under iso-diffracting condition, ultrashort vortices maintain a propagation invariant temporal shape [20]. Importantly, it has also been reported that ultrashort LG vortices and X-waves cannot carry arbitrary amount of OAM, rather there exists a lower bound to their temporal duration for given value of  $l$  [20,23]. Therefore, optical vortices with certain available spectral bandwidth cannot carry arbitrary amount of OAM. M. A. Porras et. al. has reported that for ultrashort LG vortices and X waves, the spectrum blueshifts as one moves towards the singularity and redshifts on traversing radially outward from the bright caustic [22,25]. Ultrashort optical pulses with OAM have been extensively studied in free space as well as dielectric media in space time separable case. However, to best of our knowledge space-time non-separable ultrashort optical pulse with OAM in dielectric media have been investigated yet.

In this work, we numerically investigate the dynamics of ultrashort LG vortex with PE spectrum in dispersive and nonlinear media. For modelling the propagation of the ultrashort vortex pulse, we solve the three-dimensional nonlinear Schrödinger (NLSE) equation. In ultrashort domain, however, the conventional slowly varying envelope approximation (SVEA) fails. Hence, we employ the nonlinear envelope equation (NEE) to get the deeper insights into the vortex pulse dynamics [26]. In section 2 we discuss the theory of wave equation where we see that when the temporal duration of pulse becomes comparable to the time period corresponding to the carrier frequency of the pulse, Maxwell's equations give non-separable spatio-temporal solutions. Section 3 discusses the numerical results of this paper. In this section we explore the spatio-temporal, spectral, and frequency chirp evolutions of ultrashort LG vortex across different levels of nonlinearity and propagation distances at different transverse regions of the vortex. Section 4 concludes the work.

## 2. Theory and Model:

Classically, light propagation through different kind of media is governed by Maxwell's equations. The mathematical expression of the wave equation derived from Maxwell's equations in scalar form is given by,

$$\nabla^2 E - \frac{1}{c^2} \frac{\partial^2 E}{\partial t^2} = 0, \quad (1)$$

where  $E$  is the electric field,  $c$  is the speed of light and  $\nabla^2$  is Laplacian operator. Let's consider the electric field as  $E = \psi(x, y, z, t)e^{i[\omega_0(t-z/c)]}$ , where  $\omega_0 = 2\pi/T_0$  is carrier frequency and  $T_0$  is the corresponding time period. Substituting this expression of field in equation (1) under scalar approximation, we get

$$\nabla^2 \psi - 2i \frac{\omega_0}{c} \frac{\partial \psi}{\partial z} - 2i \frac{\omega_0}{c^2} \frac{\partial \psi}{\partial t} - \frac{1}{c^2} \frac{\partial^2 \psi}{\partial t^2} = 0. \quad (2)$$

Let's consider the transformation  $t' = t - z/c$  and  $z' = z$ ,

$$\nabla_{x,y}^2 \psi - 2ik_0 \frac{\partial \psi}{\partial z} = \frac{2}{c} \frac{\partial^2 \psi}{\partial z' \partial t'}, \quad (3)$$

where  $\nabla_{x,y}^2 = \frac{\partial^2}{\partial x^2} + \frac{\partial^2}{\partial y^2}$  and  $k_0 = \frac{\omega_0}{c}$ . In equation (3) we have considered the paraxial approximation and therefore dropped  $\frac{\partial^2}{\partial z^2}$  term. Equation (3) governs the propagation of the pulsed paraxial optical beams in free space. Introducing a dimensionless variable  $\tau' = t'/T'$ , where  $T'$  is input pulse duration, we can write equation (3) as

$$\nabla_{x,y}^2 \psi - 2ik_0 \frac{\partial}{\partial z} \left[ \psi + \frac{1}{2\pi i} \left( \frac{T_0}{T'} \right) \frac{\partial \psi}{\partial \tau'} \right] = 0. \quad (4)$$

In above equation, if pulse duration  $T'$  is much longer than oscillation period  $T_0$ , the term  $\frac{T_0}{T'}$  would be very small and then second term in equation (4) can be neglected. In this condition only the factorized solutions for the above equation exist. However, if optical pulse contains only a few optical cycles, the second term in equation (4) cannot be neglected and we witness spatio-temporal coupling. A family of non-separable solutions of equation (4) in this condition exists. As a solution to eqn. (4), space-time coupled nearly gaussian pulse has already been reported in literature. However, this pulse also contains  $\exp(r^4)$  term in transverse direction, which makes the pulse in the radial direction unbounded and nonintegrable [10]. On other hand, Poisson spectrum pulse also known as power exponential (PE) pulse constitutes one of the bounded solutions to the above (3 + 1) dimensional paraxial wave equation [11,19]. The mathematical expression of the PE spectrum is given as,

$$\hat{a}_\omega = \frac{\pi}{\Gamma(\alpha+1/2)} \frac{\alpha^{\alpha+1/2}}{\bar{\omega}} \left(\frac{\omega}{\bar{\omega}}\right)^{\alpha-1/2} e^{-\frac{\omega}{\bar{\omega}}\alpha} e^{-i\varphi}, \quad (5)$$

where  $\bar{\omega}$  is the mean frequency of the pulse,  $\varphi$  is arbitrary phase and the parameter  $\alpha > 1/2$ . In the PE pulse, mean frequency  $\bar{\omega} = \frac{\int_0^\infty |\hat{a}_\omega|^2 \omega d\omega}{\int_0^\infty |\hat{a}_\omega|^2 d\omega}$  appears explicitly. The temporal shape of the PE pulse with PE spectrum is expressed as,

$$a(t) = \frac{1}{\pi} \int_0^\infty \hat{a}_\omega e^{-i\omega t} d\omega = \left(\frac{-i\alpha}{\bar{\omega}t - i\alpha}\right)^{\alpha+1/2} e^{-i\varphi}. \quad (6)$$

The shape of the PE pulse is completely determined by  $\alpha$  and scaled by  $\bar{\omega}$ . Upon increasing the value of  $\alpha$ , equation (6) resembles to Gaussian enveloped pulse with duration  $\Delta t = \sqrt{2\alpha/\bar{\omega}}$  and  $\varphi$  becomes the carrier envelope phase.

To experimentally generate ultrashort optical vortices, some technical challenges need to be overcome such as spatial, group velocity, and topological charge dispersions [27–29]. Suppose we synthesized the ultrashort optical vortices by addressing all these technical issues. The analytical complex representation of thus synthesized pulsed vortex can be given as

$$E(r, \phi, z, t') = \frac{1}{\pi} \int_0^\infty \hat{E}_\omega(r, \phi, z) e^{-i\omega t'} d\omega, \quad (7)$$

where  $\hat{E}_\omega(r, \phi, z)$  is LG beams of different frequencies and same topological charge  $l$ , which can mathematically be expressed as,

$$\hat{E}_\omega(r, \phi, z) = \hat{a}_\omega \frac{e^{-i(l+1)\Psi_\omega(z)} e^{-il\phi} \left(\frac{\sqrt{2}r}{s_\omega(z)}\right)^{|l|} \frac{e^{i\omega r^2}}{2cq_\omega(z)}}{\sqrt{1 + \left(\frac{z}{z_{R,\omega}}\right)^2}}. \quad (8)$$

The beams possess identical topological charges  $l$  and zero radial orders. In above equation, we have omitted the LG polynomial  $\left(L_p^{|l|} \left(\frac{2r^2}{s_\omega^2(z)}\right)\right)$  as for  $p = 0$ , the polynomial value will always be zero. The parameter  $\hat{a}_\omega$  is the spectral weight of LG beams. In above equations,  $t' = t - \frac{z}{c}$  is the local time,  $c$  is the speed of light in vacuum,

$q_\omega(z) = z - iz_{R,\omega}$  is the complex beam parameter,  $s_\omega(z) = s_\omega \sqrt{1 + \left(\frac{z}{z_{R,\omega}}\right)^2}$  is the beam width,  $s_\omega = \sqrt{\frac{2z_{R,\omega}c}{\omega}}$  is the waist of fundamental Gaussian beam at  $z = 0$  and  $z_{R,\omega}$  is the Rayleigh range. The complex beam parameter  $q_\omega(z)$  is generally written as

$$\frac{1}{q_\omega(z)} = \frac{1}{R_\omega(z)} + \frac{i2c}{\omega s_\omega^2(z)}, \quad (9)$$

where  $\frac{1}{R_\omega(z)} = \frac{z}{z^2 + z_{R,\omega}^2}$  represents the curvature of the phase fronts. Now integrating equation (7) with equation (5) and equation (8) at  $z = 0$  gives

$$E(r, \phi, 0, t) = \left(\frac{\sqrt{2}r}{s_\omega}\right)^{|l|} \left[ \frac{-i\left(\alpha + \frac{|l|}{2}\right)}{\bar{\omega}\left(t - i\frac{r^2}{\omega s_\omega^2}\right) - i\alpha} \right]^{\alpha + \frac{|l|}{2} + \frac{1}{2}} e^{-i\varphi}, \quad (10)$$

where  $s_\omega$  is waist of Gaussian beam at  $z = 0$ .

The dynamics of ultrashort optical pulses up to single cycle regime is described by nonlinear envelope equation (NEE). This equation is derived by resorting to the approximation known as slowly evolving wave approximation (SEWA). In this approximation not only envelope of the pulse remains unchanged during the propagation as assumed in slowly varying envelope approximation (SVEA) but also carrier envelope phase remains unchanged during the propagation. The NEE is given by [26,30],

$$\frac{\partial A}{\partial z} = \frac{i}{2k} \left(1 + \frac{i}{\omega} \frac{\partial}{\partial \tau}\right)^{-1} \nabla_\perp^2 A - \frac{i\beta_2}{2} \frac{\partial^2 A}{\partial \tau^2} + i \frac{n_2 n_0 \omega}{2\pi} \left(1 + \frac{i}{\omega} \frac{\partial}{\partial \tau}\right) |A|^2 A, \quad (11)$$

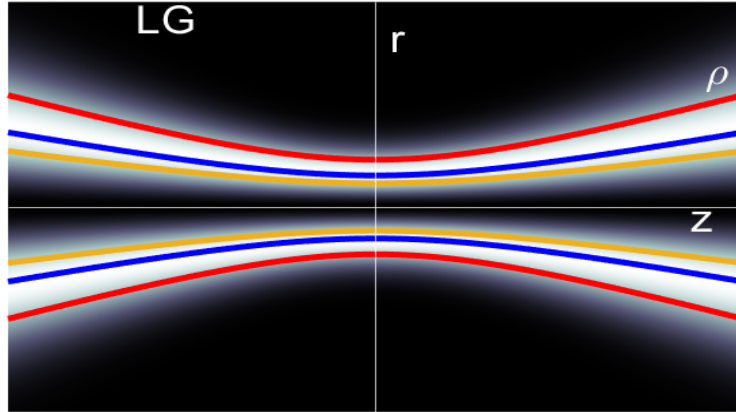
Where  $A(r, t)$  is the envelope of the optical pulse,  $\beta_2$  is the group velocity dispersion (GVD) and  $\tau = t - \frac{z}{c}$  is the local time. The presence of operator  $\left(1 + \frac{i}{\omega} \frac{\partial}{\partial \tau}\right)^{-1}$  in Laplacian term of equation (11) gives space-time focusing while its presence with Kerr nonlinear term leads to self-steeping. Owing to the cylindrical symmetry of the LG vortex, the Laplacian in equation (11) can be expressed as  $\left(\frac{\partial^2}{\partial r^2} + \frac{1}{r} \frac{\partial}{\partial r} + \frac{1}{r^2} \frac{\partial^2}{\partial \phi^2}\right)$ . To numerically solve equation (11), we have made it dimensionless by implementing the following transformations,

$$u = \frac{A}{A_0}, \rho = \frac{r}{w_0}, T = \frac{\tau}{\tau_0}, Z = \frac{z}{L_{DF}}. \quad (5)$$

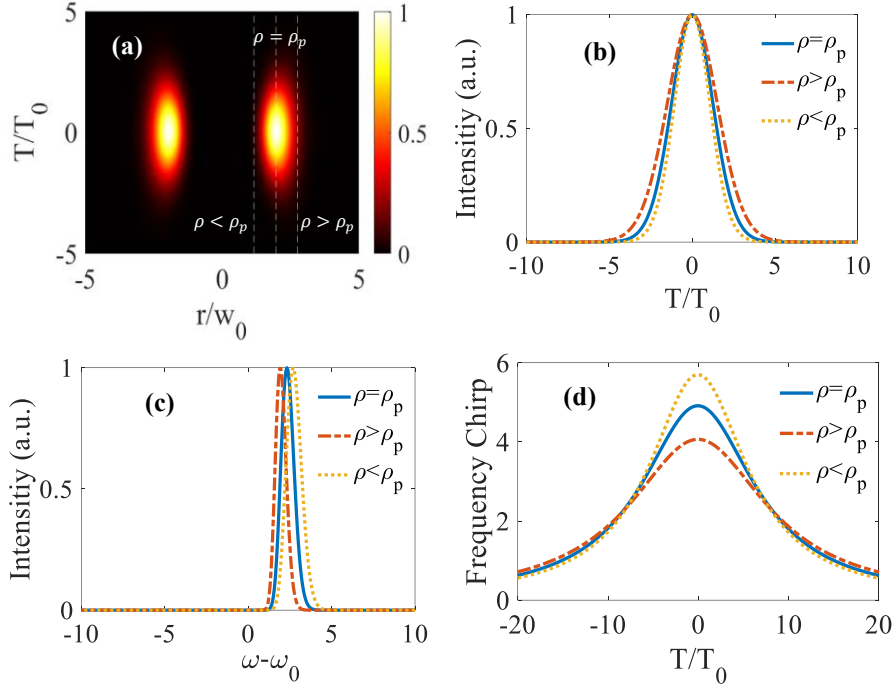
Using above transformations, where  $A_0$  is the amplitude normalization parameter,  $w_0$  is the beam waist, and  $\tau_0$  is the temporal width of the pulse. we get following dimensionless form of NEE,

$$\frac{\partial u}{\partial Z} = \frac{i}{4} \left(1 + \frac{i}{s} \frac{\partial}{\partial T}\right)^{-1} \nabla_{\perp}^2 u - i \frac{L_{DF}}{L_{DS}} \frac{\partial^2 u}{\partial T^2} + i \frac{L_{DF}}{L_{NL}} \left(1 + \frac{i}{s} \frac{\partial}{\partial T}\right) |u|^2 u, \quad (6)$$

where  $L_{DF} = \frac{kw_0^2}{2}$  is diffraction length,  $L_{DS} = \frac{\tau_0^2}{|\beta_2|}$  is dispersion length,  $L_{NL} = \left(\frac{n_0 n_2 \omega |A_0|^2}{2\pi}\right)^{-1}$  is nonlinear length and  $s = \omega \tau_0$  represents self-steeping parameter [31]. The three characteristic lengths  $L_{DF}$ ,  $L_{DS}$  and  $L_{NL}$  represent respective strengths of diffraction, dispersion, and nonlinear interactions of the LG vortex within the medium. The ratio of  $\frac{L_{DF}}{L_{NL}}$  represents the relative strength of Kerr nonlinearity. We have considered the propagation in fused silica and used following simulation parameters:  $\frac{L_{DF}}{L_{DS}} = 0.07$ ,  $s = 40$ ,  $\beta_2 = 385 \text{ fs}^2/\text{cm}$  and  $n_2 = 2 \times 10^{-6} \text{ cm}^2/\text{W}$  [26]. The *fwhm* of the input LG vortex pulse centred at  $795 \text{ nm}$  is considered to be  $30 \text{ fs}$ .



**Figure 1.** Cross section of a LG beam. Blue ( $\rho = \rho_p$ ), red ( $\rho > \rho_p$ ), and yellow ( $\rho < \rho_p$ ) curves represent revolution hyperboloids about the  $z$  axis, called here caustic surfaces of LG beam. The blue curve ( $\rho_p$ ) represents the bright caustic.



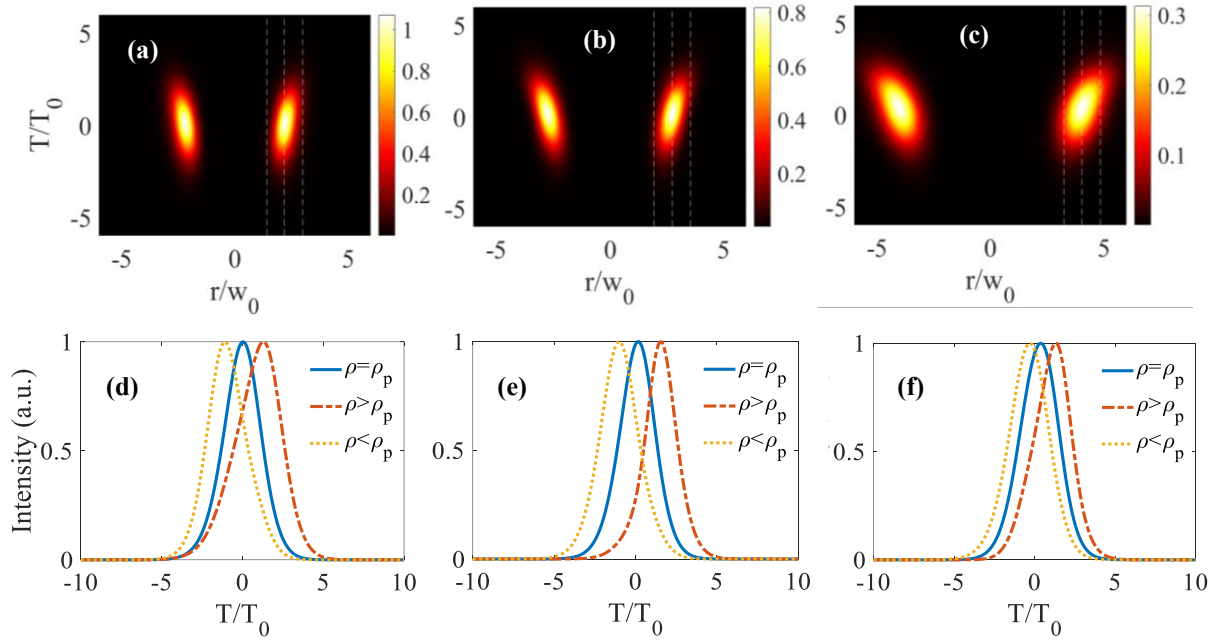
**Figure 2.** Normalized input ultrashort LG vortex for  $l = 8$ . **(a)** Spatio-temporal profile, **(b)** normalized temporal profile at different caustics, **(c)** normalized spectral profile at different caustics, and **(d)** frequencies chirp at different caustics. Blue, red, and yellow caustics are at  $\rho = 1.96$  unit,  $\rho = 2.76$  unit and  $\rho = 1.16$  unit respectively.

Figure 1 depicts the fluence distribution of the LG beam and the colorful curves on it represent the revolution hyperboloids or caustic surfaces whose revolution axis is  $z$ -axis. Figure 2 shows the spatio-temporal transverse profile of the PE pulse and its temporal (Figure 2 (b)), spectral (Figure 2 (c)) and frequency chirp (Figure 2 (d)) profiles at various caustics. In Figure 2 (b), temporal broadening is observed as one moves radially outward from the phase singularity of the pulse. In spectral profile as shown in figure 2 (c), we observe redshift and blueshift in the spectrum of the pulse as one moves respectively radially outward and towards the phase singularity from the bright caustic of the pulse. Figure 2(d) reveals the frequency chirp variation across various spatial regions of the pulse. Figure 2(d) confirms the observations of figure 2(c).

### 3. Results and Discussion

#### 3.1 Spatio-temporal Evolution

In this section, we explore the spatio-temporal dynamics of ultrashort LG vortices with PE spectrum at various propagation distance in dispersive and nonlinear medium for  $\frac{L_{DF}}{L_{NL}} = 1$ . In figure 3(a), we observe that spatio-temporal profile of the pulse becomes tilted (as compared to input as shown in figure 2 (a)) at propagation distance  $\frac{z}{L_{DF}} = 0.5$  and the tilt of the pulse increases with increase in the propagation distance (see fig. 3(b) & 3(c)). The observed tilt in the pulse comes from the spatially varying spectral distribution. As depicted in Figure 2(c), a redshift in spectrum is observed as we move radially outward from the bright caustic of the pulse and the redshifted components diffract strongly as compared to the blueshifted components. This together with the chirp profile of the input pulse (as seen in figure 2 (d)) leads to the tilt as observed in figure 3. We see that upon increasing the propagation distance, the pulse broadens both in space and time because at higher distances diffraction and dispersion comes into the play and peak intensity both in space and time decrease. In figures 3 (a-c), the three dashed vertical lines in each figure represent the three caustics. In the second row of Figure (3), we witness the temporal evolution of the pulse across different caustics of the ultrashort LG vortex. Notably, as we move radially outward ( $\rho > \rho_p$ ) from the bright caustic ( $\rho = \rho_p$ ) or approach towards the singularity ( $\rho < \rho_p$ ), an asymmetric profile is observed in the temporal domain.



**Figure 3.** Evolution of ultrashort LG vortex with PE spectrum for  $l = 8$  for  $\frac{L_{DF}}{L_{NL}} = 1$ . The first row represents the spatio-temporal evolution of the pulse, and second row depicts the temporal evolution at various caustics of LG vortex. In the first row, the three dashed vertical lines in each figure represent three caustics. In all the figures of second row, we have normalized each graph with their respective maxima. Fig (a) & fig (d) depict the evolution at  $\frac{z}{L_{DF}} = 0.5$ , fig (b) & fig (e) at  $\frac{z}{L_{DF}} = 1$  and fig (c) & fig (f) at  $\frac{z}{L_{DF}} = 2$ . At  $\frac{z}{L_{DF}} = 0.5$  blue, red, and yellow caustics are at  $\rho = 2.2$  unit,  $\rho = 3.0$  unit and  $\rho = 1.4$  unit respectively. At  $\frac{z}{L_{DF}} = 1$  blue, red, and yellow caustics are at  $\rho = 2.76$  unit,  $\rho = 3.56$  unit and  $\rho = 1.96$  unit respectively. At  $\frac{z}{L_{DF}} = 2$  blue, red, and yellow caustics are at  $\rho = 4.04$  unit,  $\rho = 4.84$  unit and  $\rho = 3.24$  unit respectively.

In figure (4), we have explored the dynamics of the pulse for higher nonlinear strength i.e., for  $\frac{L_{DF}}{L_{NL}} = 5$ . We observe in figure 4(a) that upon increasing the strength of nonlinearity the optical pulse gets compressed in space and time and that leads to splitting as observed in the second row of figure 4. The splitting in the pulse happens because of combined effect of self-focusing and normal group velocity dispersion in time domain and due to diffraction and Kerr nonlinearity in space. As shown in Figure 4(b), further propagation reveals a strong asymmetric splitting of the pulse, which is attributed to the previously discussed spatially dependent spectrum. Upon further propagation (figure 4(c)) compression at the trailing edge of the optical pulse is seen. This occurs because of diffraction and Kerr nonlinearity working together on the spatially dependent spectrum of the vortex pulse. The second row of figure (4) depicts the temporal evolution at the different caustics of the LG vortices. Notably, we observe that upon moving radially away from the bright caustics, pulse compression and splitting dominate.

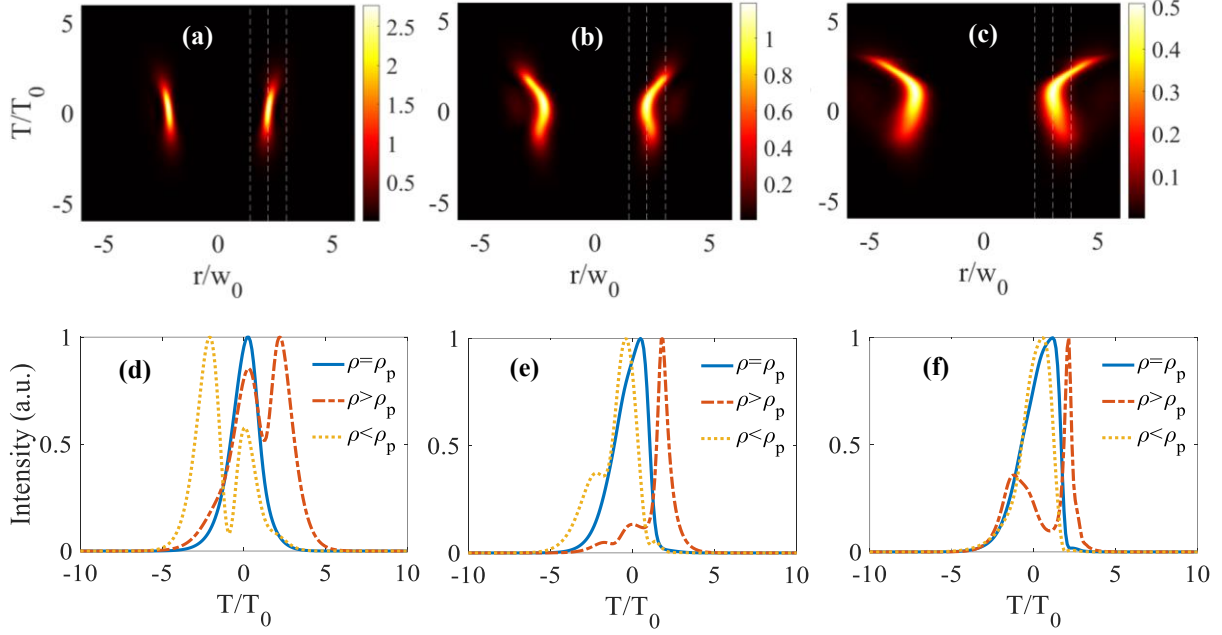


**Figure 4.** Evolution of ultrashort LG vortices with PE spectrum for  $l = 8$  with strength of nonlinearity  $\frac{L_{DF}}{L_{NL}} = 5$ . The first row represents the spatio-temporal evolution of the pulse, and the second row depicts the temporal evolution at various caustics of LG vortices. In the first row, the three dashed vertical lines in each figure represent three caustics. In all the figures of second row, we have normalized each graph with their respective maxima. Fig (a) & fig (d) depict the evolution at  $\frac{z}{L_{DF}} = 0.5$ , fig (b) & fig (e) at  $\frac{z}{L_{DF}} = 1$  and fig (c) and fig (f) at  $\frac{z}{L_{DF}} = 2$ . At  $\frac{z}{L_{DF}} = 0.5$  blue, red, and yellow caustics are at  $\rho = 2.20$  unit,  $\rho = 3.00$  unit and  $\rho = 1.40$  unit respectively. At  $\frac{z}{L_{DF}} = 1$  blue, red, and yellow caustics are at  $\rho = 2.28$  unit,  $\rho = 3.08$  unit and  $\rho = 1.48$  unit respectively. At  $\frac{z}{L_{DF}} = 2$  blue, red, and yellow caustics are at  $\rho = 3.04$  unit,  $\rho = 3.84$  unit and  $\rho = 2.24$  unit respectively.

### 3.2 Spectral Evolution

In this section, we explore the spectral evolution of ultrashort LG vortex at its different caustics. As shown in figure 5(a), for  $\frac{L_{DF}}{L_{NL}} = 1$  and  $z = 0.5L_{DF}$  as we move radially outward from the bright caustic, the ultrashort LG vortex spectrum exhibits redshift, while on moving towards the phase singularity a blueshift in spectrum is observed. Upon further propagation at  $z = L_{DF}$  (figure 5(b)), the spectra of the different spatial regions in the ultrashort LG vortex coincides with that of the bright caustic. However, upon further propagation at  $z = 2L_{DF}$ , we observe spectral characteristics opposite to what is seen in figure 5(a). Upon increasing the strength of the nonlinearity to  $\frac{L_{DF}}{L_{NL}} = 5$ , (second row of figure 5), we observe significant variation in the spectrum of the ultrashort LG vortices. We observe in figure 5(e) that at the bright caustic ( $\rho = \rho_p$ ) of the LG vortices, the spectrum has become asymmetrical. Approaching towards the singularity ( $\rho < \rho_p$ ) amplifies this asymmetry. Further, moving radially outward from the bright caustic ( $\rho > \rho_p$ ) gives minimal spectral changes. As propagation continues, nonlinear effects become increasingly pronounced, leading to complex spectral changes across different spatial regions of the LG vortex.

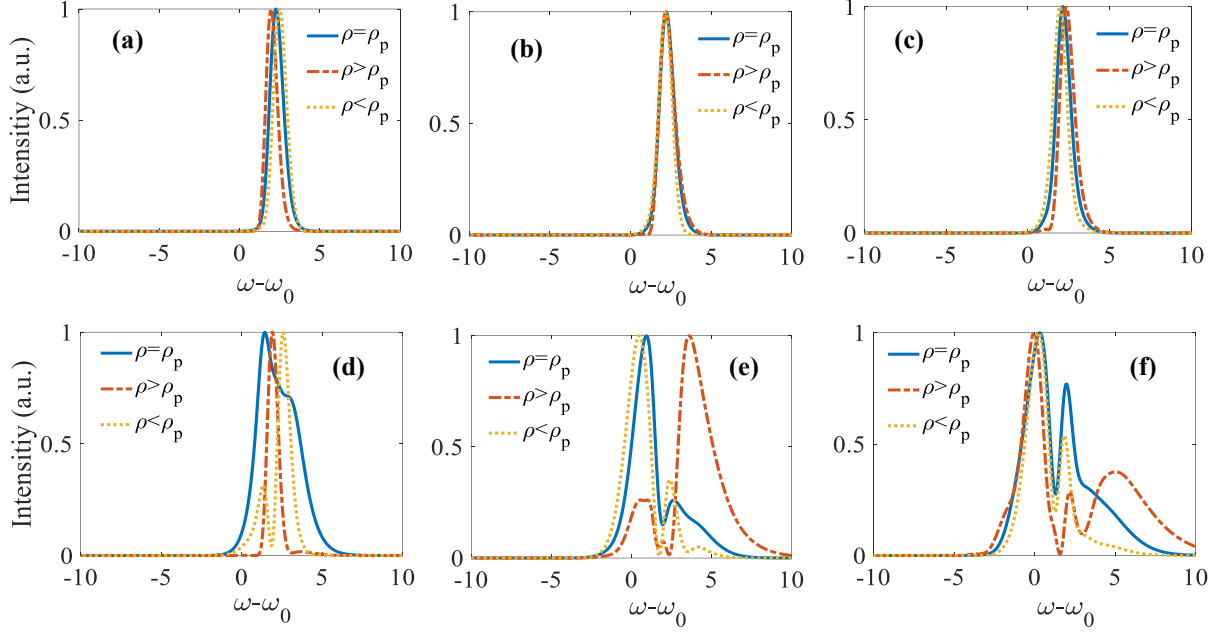


**Figure 5.** Spectral evolution of ultrashort LG vortices with PE spectrum across various spatial region for  $l = 8$ . In first column  $\frac{z}{L_{DF}} = 0.5$ , second column  $\frac{z}{L_{DF}} = 1$  and in third column  $\frac{z}{L_{DF}} = 2$ . In first row  $\frac{L_{DF}}{L_{NL}} = 1$  and in second row  $\frac{L_{DF}}{L_{NL}} = 5$ . Blue curve ( $\rho = \rho_p$ ) represents the bright caustic, red ( $\rho > \rho_p$ ) represents away from the bright caustic and ( $\rho < \rho_p$ ) represents caustic towards the singularity. In all the figures, we have normalized each graph with their respective maxima. In first row at  $\frac{z}{L_{DF}} = 0.5$  blue, red, and yellow caustics are at  $\rho = 2.2$  unit,  $\rho = 3.0$  unit and  $\rho = 1.4$  unit respectively. At  $\frac{z}{L_{DF}} = 1$  blue, red, and yellow caustics are at  $\rho = 2.76$  unit,  $\rho = 3.56$  unit and  $\rho = 1.96$  unit respectively. At  $\frac{z}{L_{DF}} = 2$  blue, red, and yellow caustics are at  $\rho = 4.04$  unit,  $\rho = 4.84$  unit and  $\rho = 3.24$  unit respectively. In second row, at  $\frac{z}{L_{DF}} = 0.5$  blue, red, and yellow caustics are at  $\rho = 2.20$  unit,  $\rho = 3.00$  unit and  $\rho = 1.40$  unit respectively. At  $\frac{z}{L_{DF}} = 1$  blue, red, and yellow caustics are at  $\rho = 2.28$  unit,  $\rho = 3.08$  unit and  $\rho = 1.48$  unit respectively. At  $\frac{z}{L_{DF}} = 2$  blue, red, and yellow caustics are at  $\rho = 3.04$  unit,  $\rho = 3.84$  unit and  $\rho = 2.24$  unit respectively.

### 3.3 Frequency Chirp Evolution

In this section, we study the evolution dynamics of frequency chirp [31] of ultrashort LG vortex at different spatial regions across the pulse. The frequency chirp of the PE pulse peaks at the pulse center. Figure 6(a) illustrates the frequency chirp of the PE pulse at  $\frac{z}{L_{DF}} = 0.5$ . Notably, we observe nominal variations in the shape of the frequency chirp while examining it at the bright caustic, radially outward from it, and toward the phase singularity. However, as we propagate further i.e. at  $\frac{z}{L_{DF}} = 1$ , the frequency chirp changes slightly for all three spatial regions. At the bright caustic (blue curve), a second peak in the frequency chirp emerges, a feature also observed for spatial region (yellow dashed curve) close to the phase singularity. As the pulse further, we observe typical signatures of the self-phase modulation on frequency chirp.



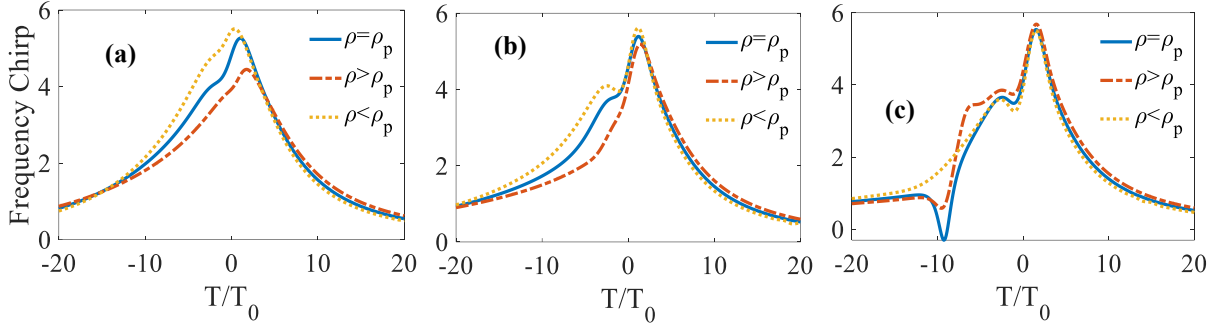


**Figure 6.** Frequency chirp evolution of ultrashort LG vortices with P. E. spectrum across various spatial region for  $l = 8$  at different propagation distances for ( $\frac{L_{DF}}{L_{NL}} = 1$ ). (a)  $\frac{z}{L_{DF}} = 0.5$ , (b)  $\frac{z}{L_{DF}} = 1$  and (c)  $\frac{z}{L_{DF}} = 2$ . In all the figures, we have normalized each graph with their respective maxima. At  $\frac{z}{L_{DF}} = 0.5$  blue, red, and yellow caustics are at  $\rho = 2.2$  unit,  $\rho = 3.0$  unit and  $\rho = 1.4$  unit respectively. At  $\frac{z}{L_{DF}} = 1$  blue, red, and yellow caustics are at  $\rho = 2.76$  unit,  $\rho = 3.56$  unit and  $\rho = 1.96$  unit respectively. At  $\frac{z}{L_{DF}} = 2$  blue, red, and yellow caustics are at  $\rho = 4.04$  unit,  $\rho = 4.84$  unit and  $\rho = 3.24$  unit respectively.

Upon increasing the strength of nonlinearity, we observe frequency chirp similar to that introduced by self-phase modulation as shown in figure 7.

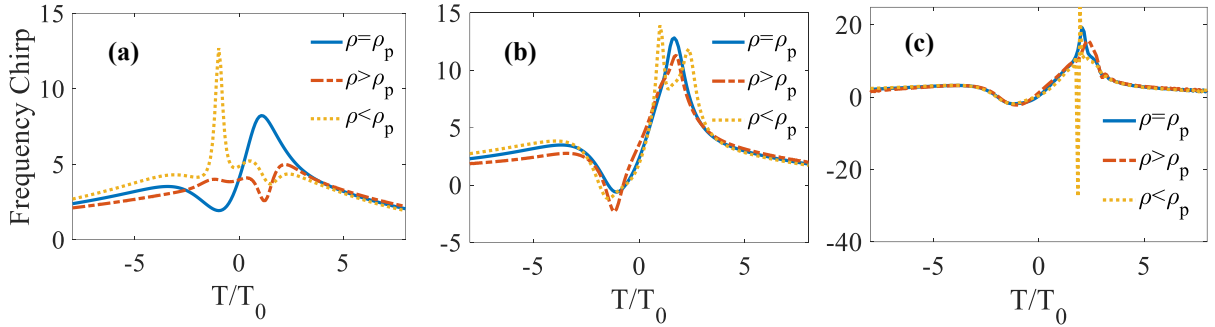


**Figure 7.** Frequency chirp evolution of ultrashort LG vortices with PE spectrum across various spatial region for  $l = 8$  at different propagation distances for ( $\frac{L_{DF}}{L_{NL}} = 5$ ). In all the figures, we have normalized each graph with their respective maxima. At  $\frac{z}{L_{DF}} = 0.5$  blue, red, and yellow caustics are at  $\rho = 2.20$  unit,  $\rho = 3.00$  unit and  $\rho = 1.40$  unit respectively. At  $\frac{z}{L_{DF}} = 1$  blue, red, and yellow caustics are at  $\rho = 2.28$  unit,  $\rho = 3.08$  unit and  $\rho = 1.48$  unit respectively. At  $\frac{z}{L_{DF}} = 2$  blue, red, and yellow caustics are at  $\rho = 3.04$  unit,  $\rho = 3.84$  unit and  $\rho = 2.24$  unit respectively.

#### 4. Conclusion

In this paper, we have studied the dynamics of space-time non-separable ultrashort LG vortex with PE spectrum in dispersive and nonlinear media at different transverse spatial regions of ultrashort vortex by employing NEE. The spatio-temporal evolution of the ultrashort vortex pulse showed asymmetry in spatio-temporal plane due to spatially dependent spectrum. Furthermore, for stronger nonlinearity and at larger propagation distances, we observed compression and splitting in the pulse in spatio-temporal plane induced by diffraction and Kerr nonlinearity. Different spatial regions of the ultrashort LG vortex witnessed different kinds of temporal asymmetric spitting. The Spectral evolution of the pulse revealed a redshifted spectrum moving radially outward from the bright caustic and a blueshifted spectrum was observed on moving towards the phase singularity at lower

nonlinearity levels and shorter distances. As propagation distance increases, the spectrum undergoes further changes, with a noticeable redshift towards the phase singularity and a blueshift radially outward from the bright caustic. Upon increasing the strength of nonlinearity and propagation distance, we observed complex spectral evolution at different spatial regions. The frequency chirp of ultrashort LG vortices with PE spectrum has also been investigated. We found that for weaker nonlinearity, the shape of the frequency chirp remains unaffected however upon increasing the strength of the nonlinearity frequency chirp resembles to that introduced by self-phase modulation.

This study may hold various applications in optical communication, compressing femtosecond LG vortices, generating supercontinuum of ultrashort LG vortices, improving temporal resolution in ultrafast spectroscopy, and OAM based tunable optical tweezers.

### Acknowledgements

Shakti Singh wishes to acknowledge the University Grant Commission (India) for the financial support. This work is supported by the research grant CRG/2022/007736 from SERB (India).

**Disclosure.** The authors declare no conflicts of interest.

**Data availability.** Data underlying the results presented in this paper are not publicly available at this time but may be obtained from the authors upon reasonable request.

### References:

1. A. M. Shaltout, K. G. Lagoudakis, J. van de Groep, S. J. Kim, J. Vučković, V. M. Shalaev, and M. L. Brongersma, Spatiotemporal light control with frequency-gradient metasurfaces, *Science* **365**, 374 (2019).
2. Z. Qiao, Z. Wan, G. Xie, J. Wang, L. Qian, and D. Fan, Multi-vortex laser enabling spatial and temporal encoding, *Photonix* **1**, 13 (2020).
3. Z. Nie, C. H. Pai, J. Hua, C. Zhang, Y. Wu, Y. Wan, F. Li, J. Zhang, Z. Cheng, Q. Su, S. Liu, Y. Ma, X. Ning, Y. He, W. Lu, H. H. Chu, J. Wang, W. B. Mori, and C. Joshi, Relativistic single-cycle tunable infrared pulses generated from a tailored plasma density structure, *Nat. Photonics* **12**, 489 (2018).
4. M. Malinauskas, A. Žukauskas, S. Hasegawa, Y. Hayasaki, V. Mizeikis, R. Buividas, and S. Juodkzasis, "Ultrafast laser processing of materials: From science to industry," *Light Sci. Appl.* **5**, e16133 (2016).
5. Y. Shen, X. Wang, Z. Xie, C. Min, X. Fu, Q. Liu, M. Gong, and X. Yuan, Optical vortices 30 years on: OAM manipulation from topological charge to multiple singularities, *Light Sci Appl* **8**, (2019).
6. Y. Shen, A. Zdagkas, N. Pappasimakis, and N. I. Zheludev, Measures of space-time nonseparability of electromagnetic pulses, *Phys. Rev. Res.* **3**, 013236 (2021).
7. S. Akturk, X. Gu, P. Bowlan, and R. Trebino, Spatio-temporal couplings in ultrashort laser pulses, *J. Opt.* **12**, 093001 (2010).
8. M. A. Porras, Diffraction effects in few-cycle optical pulses, *Phys. Rev. E* **65**, 026606 (2002).
9. E. M. Belenov and A. V. Nazarkin, Transient diffraction and precursorlike effects in vacuum, *J. Opt. Soc. Am. A* **11**, 168 (1994).
10. Z. Wang, Z. Zhang, Z. Xu, and Q. Lin, Space-time profiles of an ultrashort pulsed Gaussian beam, *IEEE J Quantum Electron* **33**, 566 (1997).
11. M. A. Porras, "Nonsinusoidal few-cycle pulsed light beams in free space," *J. Opt. Soc. Am. B* **16**, 1468 (1999).
12. L. Allen, M. W. Beijersbergen, R. J. C. Spreeuw, and J. P. Woerdman, Orbital angular momentum of light and the transformation of Laguerre-Gaussian laser modes, *Phys. Rev. E* **45**, 31 (2016).

13. S. Singh, S. K. Mishra, and A. K. Mishra, "Ring Pearcey vortex beam dynamics through atmospheric turbulence, *J. Opt. Soc. Am. B* **40**, 2287 (2023).
14. S. Singh and A. K. Mishra, "Spatio-temporal evolution dynamics of ultrashort Laguerre-Gauss vortices in a dispersive and nonlinear medium," *J. Opt.* **24**, 075501 (2022).
15. J. Wang, J. Y. Yang, I. M. Fazal, N. Ahmed, Y. Yan, H. Huang, Y. Ren, Y. Yue, S. Dolinar, M. Tur, and A. E. Willner, Terabit free-space data transmission employing orbital angular momentum multiplexing, *Nat Photonics* **6**, 488 (2012).
16. D. G. Grier, A revolution in optical manipulation, *Nature* **424**, 810 (2003).
17. A. Jesacher, S. Fürhapter, S. Bernet, and M. Ritsch-Marte, Shadow effects in spiral phase contrast microscopy, *Phys. Rev. Lett* **94**, 233902 (2005).
18. G. Molina-Terriza, J. P. Torres, and L. Torner, Management of the Angular Momentum of Light: Preparation of Photons in Multidimensional Vector States of Angular Momentum, *Phys. Rev. Lett.* **88**, 013601 (2002).
19. M. A. Porras, Effects of the Coupling between the Orbital Angular Momentum, and the Temporal Degrees of Freedom in the Most Intense Ring of Ultrafast Vortices, *Appl. Sci.* **10**, 1957 (2020).
20. M. A. Porras, Upper Bound to the Orbital Angular Momentum Carried by an Ultrashort Pulse," *Phys. Rev. Lett.* **122**, 123904 (2019).
21. Y. Fang, Z. Guo, P. Ge, Y. Dou, Y. Deng, Q. Gong, and Y. Liu, "Probing the orbital angular momentum of intense vortex pulses with strong-field ionization," *Light. Sci. Appl.* **11**, (2022).
22. M. A. Porras, C. Conti, and C. Conti, Couplings between the temporal and orbital angular momentum degrees of freedom in ultrafast optical vortices, *Phys. Rev. A* **101**, 63803 (2020).
23. M. Ornigotti, C. Conti, and A. Szameit, Effect of Orbital Angular Momentum on Nondiffracting Ultrashort Optical Pulses, *Phys. Rev. Lett.* **115**, 100401 (2015).
24. M. A. Porras, "Ultrashort pulsed Gaussian light beams," *Phys. Rev. E* **58**, 1086 (1998).
25. M. A. Porras, "Effects of orbital angular momentum on few-cycle and sub-cycle pulse shapes: coupling between the temporal and angular momentum degrees of freedom," *Opt. Lett.* **44**, 2538 (2019).
26. J. K. Ranka and A. L. Gaeta, Breakdown of the slowly varying envelope approximation in the self-focusing of ultrashort pulses, *Opt. Lett.* **23**, 244 (1998).
27. K. Bezuharov, A. Dreischuh, G. G. Paulus, M. G. Schätzel, and H. Walther, Vortices in femtosecond laser fields, *Opt. Lett.* **29**, 1942 (2004).
28. I. Zeylikovich, H. I. Sztul, V. Kartazhev, T. Le, and R. R. Alfano, Ultrashort Laguerre-Gaussian pulses with angular and group velocity dispersion compensation, *Opt. Lett.* **32**, 2025 (2007)
29. Y. Tokizane, K. Oka, and R. Morita, "Supercontinuum optical vortex pulse generation without spatial or topological-charge dispersion," *Opt. Express* **17**, 14517 (2009).
30. T. Brabec and F. Krausz, Nonlinear optical pulse propagation in the single-cycle regime, *Phys. Rev. Lett.* **78**, 3282 (1997).
31. G. P. Agrawal, *Nonlinear Fiber Optics*, Academic Press, Fifth Edition (2013).